Cite this article
Adinolfi M, Rianna G, Mercogliano P, Maiorano RMS and Aversa S
Behaviour of energy piles under climate-change scenarios: a case study in Southern Italy.
Environmental Geotechnics,
https://doi.org/10.1680/jenge.19.00093

Research Article
Paper 1900093
Received 15/04/2019; Accepted 25/03/2020

Keywords: energy/environmental engineering/piles & piling

Environmental Geotechnics

ice Publishing

Behaviour of energy piles under climate-change scenarios: a case study in Southern Italy

Marianna Adinolfi PhD
Researcher, Regional Models and Geo-Hydrological Impacts Division, Euro-Mediterranean Center on Climate Change Foundation, Capua, Italy (Orcid:0000-0002-8341-2742) (corresponding author: marianna.adinolfi@cmcc.it)

Guido Rianna PhD
Researcher, Regional Models and Geo-Hydrological Impacts Division, Euro-Mediterranean Center on Climate Change Foundation, Capua, Italy (Orcid:0000-0003-0956-4243)

Paola Mercogliano MSc
Researcher, Regional Models and Geo-Hydrological Impacts Division, Euro-Mediterranean Center on Climate Change Foundation, Capua, Italy; METE Laboratory, Italian Aerospace Research Centre, Capua, Italy (Orcid:0000-0001-7236-010X)

Rosa Maria Stefania Maiorano PhD
Assistant Professor, Department of Engineering, University of Napoli Parthenope, Naples, Italy (Orcid:0000-0001-7452-9001)

Stefano Aversa PhD
Professor, Department of Engineering, University of Napoli Parthenope, Naples, Italy (Orcid:0000-0002-0263-757X)

Energy geostructures are renewable-energy solutions that are strongly recommended as mitigation policy tools for facing the issue of global warming. Meanwhile, ongoing climate changes influence society through impacts on cities and structures, potentially affecting their effectiveness and functionalities and requiring assessments regarding adaptation. With that aim, the present research considers the future behaviour (until 2100) of an energy pile installed in Naples, Italy, supposing the influences of climate change on underground soil temperature and energy demand. The key points are that (*a*) future projections of air temperature and ground temperature highlight increases from 2 to 4°C in Naples, (*b*) future energy demand for indoor comfort goes to reducing the heating need of the building and increasing the cooling one and (*c*) the variations in the behaviour of the energy pile due to climate change on the long-term horizon (with increasing heating potential, thus reducing the cooling potential of the energy pile–soil system) are addressed mainly by the initial temperature of the ground. The outcomes, obtained with a thermo-hydro-mechanical model, give key insights into the geotechnical performance and thermal exchange, from a climate-change perspective, to support the future development of energy geostructures and design strategies.

Notation

A_0	amplitude of the sinusoidal wave in soil temperature propagation
$\boldsymbol{b}$	volume external force vector due to the gravity loads
c	soil specific heat capacity
c_s	solid-skeleton specific heat capacity
c_w	water specific heat capacity
$\boldsymbol{D}^e$	elastic stiffness tensor
d	damping depth in soil temperature propagation
$\boldsymbol{I}$	second-order unit tensor
$\boldsymbol{K}$	hydraulic conductivity tensor
p	pore water pressure
T_{2m}	yearly average value of the near-surface (2 m) air temperature
T_{ave}	mean yearly air temperature
T_c	temperature inside the probes during cooling
T_h	temperature inside the probes during heating
T_m	outside daily mean temperature
T_{ref}	initial soil temperature
$T(t)$	thermal load imposed along the heat exchanger
T^*, T^{**}	comfort temperature indoor (18°C in winter and 21°C in summer, respectively)
t	time
$\boldsymbol{v}$	relative velocity vector
α	thermal diffusivity of soils
α_s	volumetric axial thermal expansion coefficient
β_{sw}	volumetric thermal expansion of the bi-phase mass
ΔT	temperature variation
$\boldsymbol{\varepsilon}$	strain tensor
$\boldsymbol{\varepsilon}_{pl}$	plastic strain tensor
$\boldsymbol{\varepsilon}^T$	thermal strain tensor
ε_{vol}	volumetric strain
$\boldsymbol{\lambda}_{eff}$	thermal conductivity tensor of the soil
$\boldsymbol{\sigma}$	total stress tensor
ρ	soil density
$(\rho c)_{eq}$	volumetric heat capacity of saturated soil
ω	radial frequency corresponding to the period duration of temperature oscillations
∇^2	Laplace operator

Introduction

Climate change (CC) is one of the greatest economic, social and environmental challenges to which the world has been exposed (IPCC, 2014). In 2015, the UN unveiled a roadmap on how to face CC in the coming years. In the Paris Agreement, the two pillars of coping with CC are mitigation (i.e. reducing the sources or enhancing the sinks of greenhouse gases (GHGs)) and adaptation (i.e. adjusting to the actual or expected climate and its effects).

Governments and international organisations are trying very hard to (*a*) identify the most effective ways to reduce the emissions of GHGs and (*b*) adequately address the potential impacts of CC and solutions in different sectors. Energy sector is pivotal: in addition to energy conservation measures, renewable-energy sources are an extraordinarily effective means of reducing emissions. Considered one of the most promising renewable technologies, geothermal energy has attracted remarkable interest in recent years. Ground-source heat pump (GSHP) systems exploit shallow ground as a geothermal energy source, although they do not completely offset the electrical energy input that is required to drive the GSHP when heating and cooling a residential or commercial building. Among GSHP systems, energy geostructures (EGs) have recently grown exponentially as geotechnical infrastructure elements (e.g. piles, piled or diaphragm walls, tunnels, metro stations), supplying both structural and geothermal roles. However, the design, maintenance and performance of EGs require potential CC-induced variations to be accounted for carefully, all the more so because the economic advantages of installing EGs are enjoyed only after many years. To date, by far the most common EGs have been energy piles (EPs). EPs are foundation elements in concrete integrated with probes in polyethylene that transport circulating fluid to the GSHP, thereby extracting geothermal energy from the ground.

Several studies have reviewed the impact of thermal loads on the thermo-mechanical behaviour of a single EP by means of full-scale in situ tests (Badenes *et al*., 2017; Bourne-Webb *et al*., 2009; De Santiago *et al*., 2016; Laloui *et al*., 2006). Based on the available experimental data, advanced numerical techniques have been developed and validated for use as prediction tools to investigate further configurations as either EP groups or complex EGs whose physical testing is either impossible or too expensive. The main tool for analysing coupled problems with complicated domains and boundary conditions is the finite-element method (Adinolfi *et al*., 2016, 2018; Di Donna and Laloui, 2015; Laloui *et al*., 2006; Olgun *et al*., 2015; Ozudogru *et al*., 2015; Rotta Loria and Laloui, 2017; Suryatriyastuti *et al*., 2012).

A review of the literature (Bourne-Webb *et al*., 2019; Sani *et al*., 2019) shows that the EP operating principle is energy transfer among ground, concrete and fluid flowing inside the probes. Consequently, because an EP acts simultaneously as a bearing structure and a heat-exchange element, it is subjected to not only the mechanical load of the overlying structure but also variations in the temperature of the heat-transport fluid, depending on the soil temperature and the energy demand (ED) of the building. Temperature exchanges cause the volumes of concrete piles to vary: expansion when the piles are heated and contraction when they are cooled (Rotta Loria and Laloui, 2018). Moreover, temperature exchanges influence the thermal behaviour of the surrounding soil, depending on its characteristics, thereby affecting the mechanical behaviour of both the foundation and the overlying structure. This complex behaviour, involving EPs, the surrounding soil and the overlying structure, could vary over a long time horizon. Both (*a*) the thermal exchange between an EP and the soil and (*b*) the consequent geotechnical performance are governed by two main factors that are linked strongly to external weather forcing and thus to CC. The first factor is the temperature of the ground that is being used as an energy source. Although the soil temperature depends on the thermal properties and soil state (porosity, water content), below 15–20 m, it is relatively constant throughout the year and is close to the average air temperature (Brandl, 2006; Burger *et al*., 1985; Suryatriyastuti *et al*., 2012). Consequently, in view of global warming and more specifically an increasing near-surface air temperature, ground temperatures are expected to rise in the twenty-first century (see the section headed 'High-resolution climate simulations and projections of air temperature'), thereby affecting the thermal and geotechnical performances of geo-energy systems. The second factor is the ED, which is influenced strongly by CC in terms of the energy consumption in heating and cooling the building. Despite the remarkable scientific interest in EP technology, there has been no investigation to date into how variations induced by CC could affect its performance (e.g. energy efficiency, structural stresses). As such, the present study provides insights into many aspects of how CC could affect EPs.

The present work begins with very high-resolution climate projections, up to 2100 under different scenarios, being used to provide future projections of near-surface air temperature and consequently the influences on soil temperatures for Naples (Southern Italy). Next, an approach to quantifying the future ED is proposed. The projections of near-surface air temperature are used as inputs to evaluate future potential variations in the behaviour of an operating EP. As a pilot case, the numerical approach detailed by Adinolfi *et al*. (2018) is used: existing results regarding the current behaviour of the same pile are compared with the predicted behaviour in future scenarios. Then, considering the environmental, geotechnical and thermal aspects, the advantages and disadvantages in the use of EP are laid out over a long time horizon to support future developments of this technology.

High-resolution climate simulations and projections of air temperature

Future projections regarding the area of interest exploit high-resolution climate simulations performed over Italy for 1971–2100 by Bucchignani *et al*. (2016). The main elements that are generally included in the simulation chains that are usually used to estimate future variations are recalled briefly in Appendix 1. The adopted method is summarised in the following.

- The Representative Concentration Pathway (RCP) scenarios that the global climate model (GCM) uses are RCP 4.5 (the midway-stabilisation scenario) and RCP 8.5 (the highest-concentration scenario).
- The GCM is the Euro-Mediterranean Center on Climate Change Climate Model (CMCC-CM) (Scoccimarro *et al*., 2011), a coupled atmosphere–ocean general circulation model whose atmospheric component is the fifth-generation European Centre Hamburg Model (Echam5), with a

horizontal resolution of 0.75° (~85 km) driven by the RCP 4.5 and RCP 8.5 scenarios.
- The regional climate model is the Consortium for Small-scale Modeling Model in Climate Mode (Cosmo-CLM) (Rockel *et al*., 2008), with a configuration optimised over the Italian area by Bucchignani *et al*. (2016), downscaling the results at a horizontal resolution of 0.0715° (~8 km).
- Empirical quantile mapping (Gudmundsson *et al*., 2012) is used for bias-adjusting the temperature data, where the functions regulating the fitting between observed and estimated temperature quantiles are empirical (non-parametric) (Villani *et al*., 2015; Zollo *et al*., 2014).

Figure 1(a) shows the yearly average of the mean near-surface air temperature (T_{2m}) as provided by bias-corrected regional climate simulations from 1971 to 2100 under RCP 4.5 and RCP 8.5 and the available observations as provided by Hydrological Yearbooks (1971–2000). The simulated and observed data refer to the area of Naples. Monotonically increasing trends are tested for statistical significance using the non-parametric Mann–Kendall test, while the slope of a linear trend is estimated using the non-parametric Sen method, which is recognised as an effective means of minimising the potential effect of outliers.

Climate projections confirm a general warming in Naples, with linear trends of around 2.8 and 5.0°C per century for RCP 4.5 and RCP 8.5, respectively (with a significance of 0.01% according to the Mann–Kendall test). The temperature increases follow the same trends in a seasonal analysis (December–January–February (DJF) in Figure 1(b) and June–July–August (JJA) in Figure 1(c)). In the overlapping period between model and observed data, the bias-corrected results and the observed data are effectively close.

Soil temperature profiles for past, current and future time spans

Soil temperature drives the magnitude of the heat exchange between an EP and the surrounding medium (Di Donna and Barla, 2016). The physical processes that govern the complex heat transfer through the soil are mainly conduction and convection controlled by the thermal diffusivity α (Hillel, 2012). Accordingly, the variations in time and along the soil profile can be approximated by a sinusoidal behaviour – namely

$$1. \quad T(z,t) = T_{ave} + A_0 e^{-z/d}[\sin(\omega t - z/d)]$$

where T_{ave} is the mean yearly air temperature, equivalent to the average temperature of the surface if radiation effects and geothermal temperature gradient are neglected (Brandl, 2006); A_0 is the amplitude of the sinusoidal wave; and ω is the radial frequency. The damping depth d represents the depth at which the surface temperature amplitude is reduced by 1/e, related to the thermal diffusivity α and the soil state properties. At seasonal scale, variations of the soil temperature profile in Naples are simulated in Figure 2, accounting for the stratification of the pilot case in the paper by Adinolfi *et al*. (2018). The soil properties used for the analyses refer to the prevalent stratum in tuff (thermal conductivity 1.48 (W/m)/K; specific heat capacity 850 (J/kg)/K; soil density 1700 kg/m^3), and the thermal properties of the thin shallower stratum are neglected.

The subplots in Figure 2(a) show the soil temperature profiles for the baseline period of 1981–2010 and the scenarios for 2071–2100 under RCP 4.5 and RCP 8.5. The yearly average value of T_{2m} is used as the value of T_{ave} in Equation 1. The baseline ground temperature profiles vary from 9°C in winter (DJF) to 25°C in summer (JJA) with an average ground temperature of 16.9°C (Figure 2(a)),

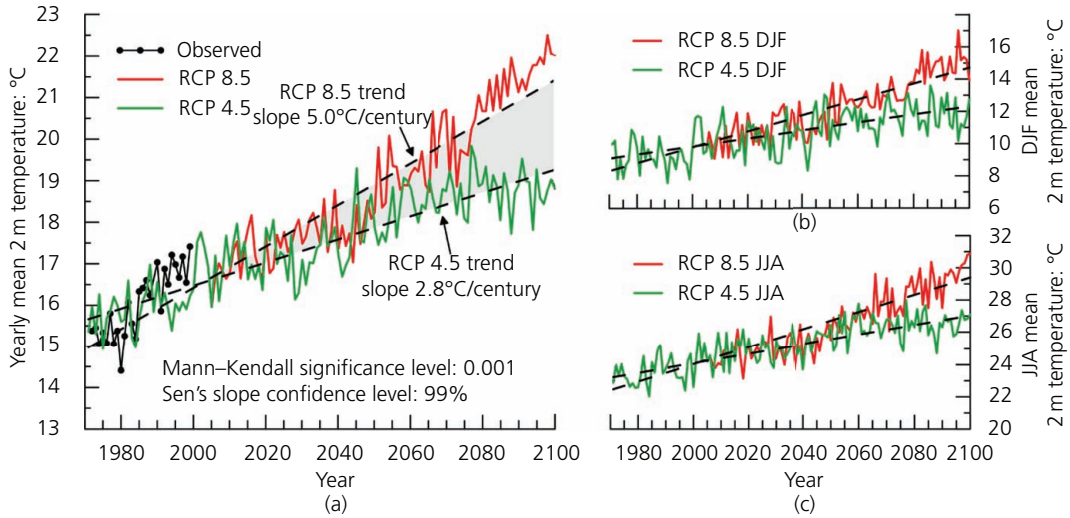

Figure 1. Mean near-surface air temperature (T_{2m}) in Naples for 1971–2100 with RCP 4.5 and RCP 8.5: (a) yearly average and observed values; (b) average in winter (December–January–February (DJF)); (c) average in summer (June–July–August (JJA))

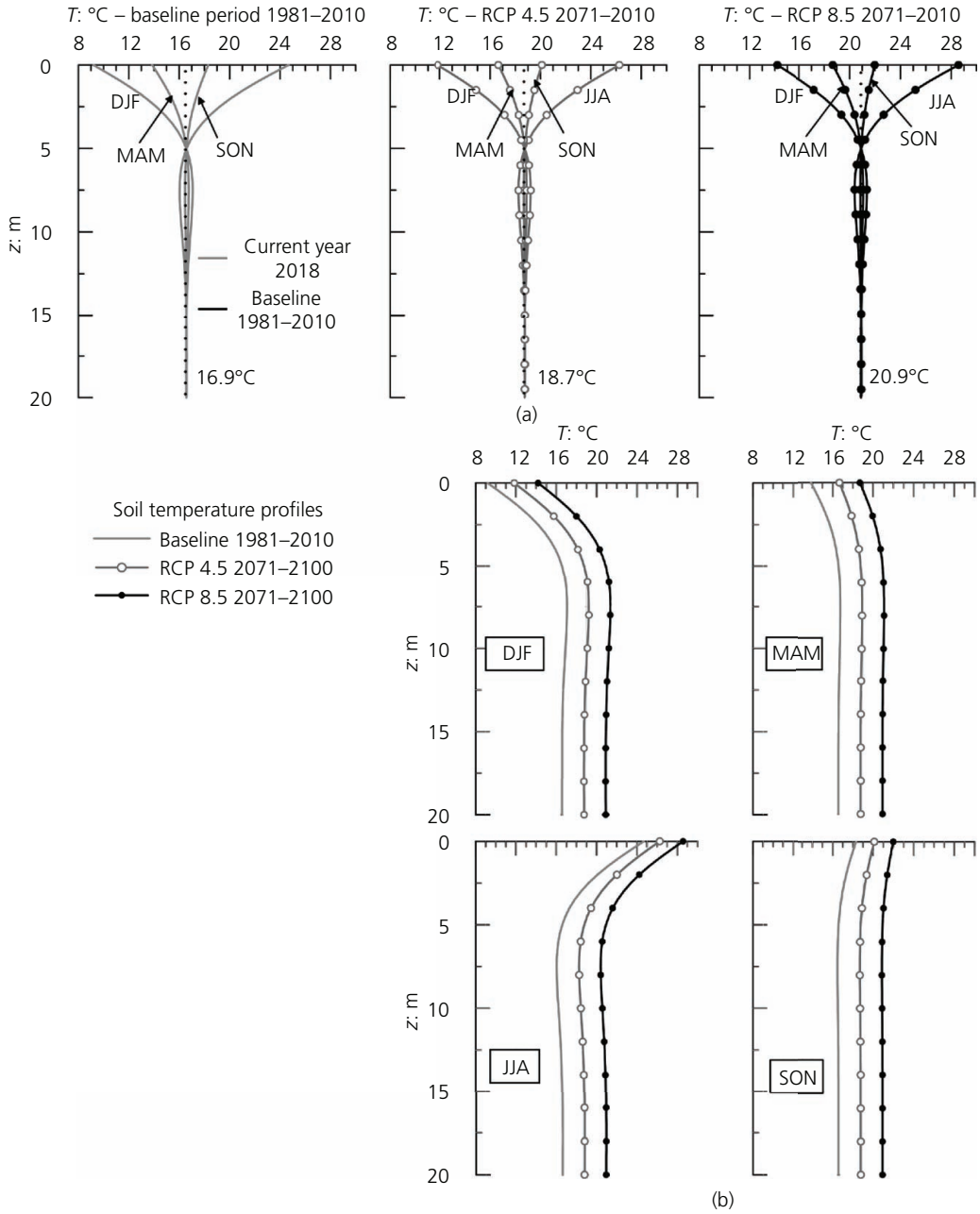

Figure 2. Soil temperatures in Naples related to the baseline period 1981–2010 and 2071–2100 with RCP 4.5 and RCP 8.5 scenarios: (a) yearly soil temperature profiles with depth; (b) seasonal profiles. DJF, December–January–February; MAM, March–April–May; JJA, June–July–August; SON, September–October–November

consistent with those adopted by Adinolfi *et al.* (2018) for steady-state conditions. Under the RCP 4.5 scenario, the ground temperature profiles vary from 12°C in winter (DJF) to 26°C in summer (JJA) with an average ground temperature of 18.7°C, while under RCP 8.5, the range of temperature profiles varies from 14°C in winter (DJF) to 29°C in summer (JJA) with an average ground temperature of 20.9°C. Moreover, Figure 2(a) shows that the soil temperature fluctuates according to the surface temperature and that the amplitude decreases with depth because of the thermal inertia of the soil. The fluctuation disappears at a depth of 12 m, and the temperature remains constant close to the average air temperature (Brandl, 2006; Burger *et al.*, 1985; Suryatriyastuti *et al.*, 2012). In Figure 2(b), the soil temperature of the uppermost layer reaches its minimum and maximum values during winter (DJF) and summer (JJA), respectively, while during autumn (September–October–November) and spring (March–April–May), the soil temperature is almost constant. Analysing the seasonal soil profiles leads to the following conclusions. Following the climate projections over the twenty-first

century with the Intergovernmental Panel on Climate Change (IPCC) RCP 4.5 and RCP 8.5 scenarios, the ground temperature in Naples is expected to increase by around 2 and 4°C, respectively, relative to the baseline period. Although fluctuations in soil temperature should be accounted for to model correctly the thermal performance of shallow geothermal applications such as EPs (Jeong *et al*., 2014; Suryatriyastuti *et al*., 2012), in the proposed case, a constant reference soil temperature is assumed (Bourne-Webb *et al*., 2009; Laloui *et al*., 2006) that equals the average value for the baseline period and the two RCP scenarios. This assumption, also used in the analyses by Adinolfi *et al*. (2018), is justified fundamentally by the presence of the concrete slab, simulated as a distributed load, over the pile and the whole domain, which prevents temperature fluctuations. Many studies (Bayer *et al*., 2016; Rivera *et al*., 2017; Zhang *et al*., 2015) suggest that urban heating can be crucial for the ground thermal regime and that if a building or other structure is present at the ground surface, then alternative boundary conditions should be considered in numerical studies (Bourne-Webb *et al*., 2016; Menberg *et al*., 2013; Oke *et al*., 2017). The literature proposes different approaches regarding the surface temperature condition: some studies (Brandl, 2006; Jeong *et al*., 2014; Olgun *et al*., 2015; Sani *et al*., 2019; Suryatriyastuti *et al*., 2012) assume that the ground surface temperature is governed by the daily mean air temperature, whereas others (Di Donna and Laloui, 2015; Dupray *et al*., 2014; Gawecka *et al*., 2018; Salciarini *et al*., 2012, 2015) assume a constant temperature at the upper boundary regulated by the overlying structure. The present study is based on the former approach, although additional analyses are proposed in Appendix 3 to account for the presence of the building.

Assessment of future ED

The ED of a building, in terms of requirements for air-conditioning in summer and heating in winter, reflects the outdoor temperature. However, the ED is a non-linear function of temperature (Lee and Chiu, 2011), and a common strategy for capturing this relationship is to use degree-day indices at daily resolution (Scapin *et al*., 2016). A degree day is a fictitious quantity that is defined as the deviation in degrees Celsius from a reference temperature (UK Met Office, 2013). Degree days are the number of degrees by which the outdoor temperature (T_m) is above or below a threshold (T^* = 18°C for winter and T^{**} = 21°C for summer). In other words, they represent the amount of heat that has to be pumped out from a building during summer – cooling degree days (CDD) – or added to a building during winter – heating degree days (HDD) – to maintain a comfortable indoor temperature. The calculations are as follows

$$\mathrm{HDD} = \max(T^* - T_m, 0) T^* = 18°\mathrm{C} \quad \text{if } T_m < 15°\mathrm{C} \tag{2}$$

$$\mathrm{CDD} = \max(T_m - T^{**}, 0) T^{**} = 21°\mathrm{C} \quad \text{if } T_m > 24°\mathrm{C} \tag{3}$$

To define the comfort zone, T^* and T^{**} follow the Eurostat–Joint Research Centre/Monitoring Agricultural Resources (JRC/Mars) indications (Spinoni *et al*., 2015). Figure 3(a) shows the monthly temperature values for the reference period and the future (2071–2100) under RCP 4.5 and RCP 8.5, and Figure 3(b) shows the associated HDD and CDD values accumulated over a monthly period and averaged over the baseline.

The HDD value decreases if comparing the periods 1981–2010 and 2071–2100, and it reaches its minimum values under RCP 8.5; the opposite happens for the CDD value. To quantify the relationship between HDD/CDD and building ED, a novel approach is proposed in this work, optimised for this case study.

In the framework of EP technology, the ED corresponds to extracting energy from the ground in winter (i.e. the heating demand of the building and the cooling phase for the pile–soil system) and injecting energy in the ground in summer (i.e. the cooling demand of the building and the heating phase for the pile–soil system). During the extraction and injection phases, the temperatures of the fluid circulating inside the heat exchanger into the EP are set as 10 and 28°C, respectively.

Figure 3(c) involves the ED from the paper by Adinolfi *et al*. (2018), which lasts for 400 d and comprises (*a*) 46 d with neither injection nor extraction but only an applied mechanical load, (*b*) 136 d of extraction or the cooling phase of the pile–soil system, (*c*) 61 d of recovery with no heat exchange and (*d*) 122 d of injection or the heating phase of the pile–soil system. The energy extraction lasts from 15 November to 31 March, while the energy injection starts on 1 June and lasts for 4 months until 30 September.

More reliable criteria for assessing the ED of a building for a future time span involve the evaluation of thresholds (Figure 3(b)).

- HDD or CDD is less than 70. The temperature inside the heat exchanger is set to the soil temperature (T_{ref}), which means that the building requires no energy for conditioning or heating and the GSHP system is turned off with no extraction/injection from/into the ground.
- HDD or CDD is between 70 and 130. The GSHP system is turned off (and the temperature is set to T_{ref}) for half a month, while for the other half, the temperatures inside the probes are set to 10°C (T_c) and 28°C (T_h) during cooling and heating periods, respectively.
- HDD or CDD is greater than 130. The GSHP is turned on for the whole month, and the temperature inside the probes is T_c or T_h.

The results obtained with this approach are compared for the past, current and future periods in Figure 3(c). The ED related to RCP 4.5 comprises (*a*) 46 d with neither injection nor extraction but only an applied mechanical load, (*b*) 136 d of extraction or the

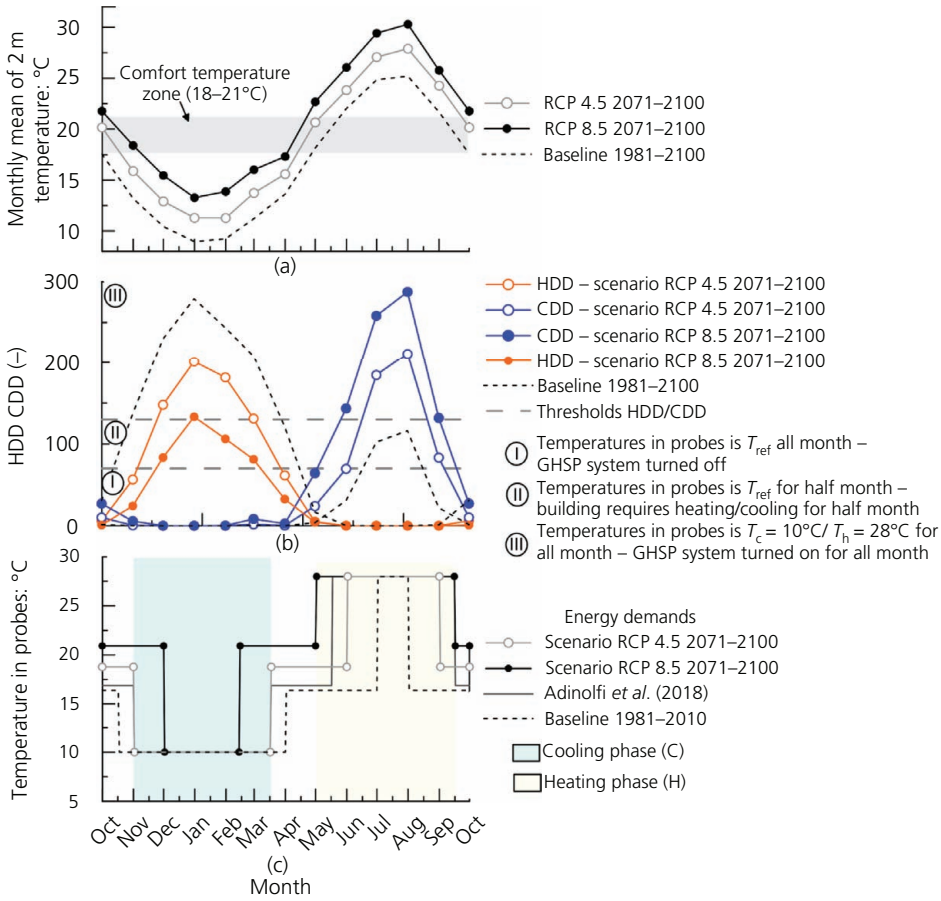

Figure 3. Analyses of yearly mean over the baseline period 1981–2010 and future projections for 2071–2100 with RCP 4.5 and RCP 8.5 scenarios: (a) monthly mean of T_{2m} and comfort zone; (b) HDD and CDD and thresholds on degree days; (c) ED in terms of temperature inside heat exchanger with cooling and heating phases

cooling phase, (*c*) 75 d of recovery with no heat exchange and (*d*) 90 d of injection in the heating phase of the pile–soil system. The energy extraction lasts from 15 November to 31 March, while energy injection starts on 15 June and lasts for 3 months until 15 September.

The ED related to RCP 8.5 comprises (*a*) 76 d with neither injection nor extraction but only an applied mechanical load, (*b*) 75 d of extraction or the cooling phase, (*c*) 75 d of recovery and (*d*) 135 d of injection during the heating phase. The energy extraction lasts from 15 December to 28 February, while energy injection starts on 16 May and lasts for four and half months until 30 September.

Note that the energy extraction during winter (cooling phase for the pile–soil system) lasts for less time, particularly with RCP 8.5. Contrariwise, the ED of conditioning the building during summer, corresponding to the heating phase of the pile–soil system, increases, particularly with RCP 8.5. Note also that the ED from the paper by Adinolfi *et al*. (2018) could result in erring on the side of safety, particularly during summer.

The main outcome of this analysis emphasises the development of EPs and, in general, EG technologies that in future projections are expected to satisfy the increasing conditioning requirements of buildings.

Performance of an EP in Naples

The present study focuses on a single EP in Naples involving a superficial layer of a pyroclastic soil known as 'pozzolanas' that overlies a deep stratum of saturated yellow tuff. The material properties are taken from the paper by Adinolfi *et al*. (2018) and reported in Figure 4. The EP works with (*a*) a mechanical load of 1000 kN on the pile head, (*b*) a distributed load due to the weight of a concrete slab (modelled as a uniformly distributed load of 17 kPa at the ground level) and (*c*) a thermal load imposed by the temperature of the injected fluid (taken as constant along the probes) given by a long-term 400 d ED under different scenarios. The numerical model and results are discussed in the following.

Numerical model and initial and boundary conditions

A thermo-hydro-mechanical (THM) coupled formulation is employed with governing equations and assumptions detailed in

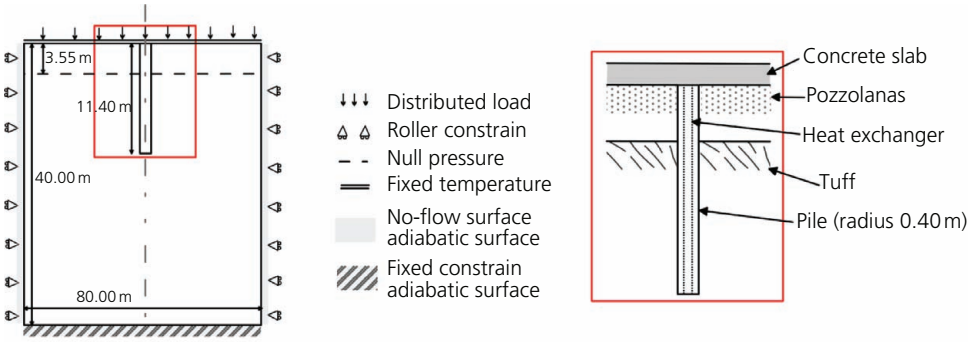

	Pile	Pozzolanas	Tuff	Measurement units
Unit weight, γ	24	17	17	(kN/m^3)
Young's modulus, E	40 000		1500	(MPa)
Poisson's ratio, ν	0.200	0.300	0.25	
Thermal expansion, α_s	8.5×10^{-6}	4×10^{-5}	4×10^{-5}	K^{-1}
Thermal conductivity, λ_{eff}	2.33	2.30	1.48	(W/m)/K
Specific heat capacity, c	960	800	850	(J/kg)/K
Permeability, k	—	1.4×10^{-6}	4×10^{-7}	(m/s)
Porosity, n	—	0.525	0.550	
Cohesion, c'	—	20	1000	(kPa)
Friction angle, ϕ'	—	38	28	(°)

Figure 4. Numerical model: analysis domain with geometrical features, boundary conditions (mechanical, thermal and hydraulics); magnified region of EP and soil layers; material properties

Appendix 2 and in the paper by Adinolfi *et al.* (2018). The numerical model is solved using the finite-element method with a two-dimensional axially symmetric computational domain and the boundary conditions of Figure 4. The EP exhibits a linear thermo-elastic behaviour, while the soil behaves as a linear elastic–perfectly plastic material.

As evaluated in Figure 3(c), the ED is imposed as a thermal load $T(t)$ along the heat exchanger, neglecting its thermal properties, which is modelled as a vertical cut line of the pile domain located at a distance of half the radius from the pile axis (Figure 4). The temperature inside the probe is T_c = 10°C or T_h = 28°C, which are conventional values for the operation of the GSHP system and are held constant into the future. The initial soil temperature is T_{ref}.

Three simulations were performed under a 400 d load: the first uses the ED from the paper by Adinolfi *et al.* (2018) and T_{ref} = 16.9°C as the initial soil temperature, the second uses RCP 4.5 as the ED and T_{ref} = 18.7°C and the third uses RCP 8.5 and T_{ref} = 20.9°C. Given the geotechnical design of EPs, the interest in studying the soil deformation near the foundations is the need to verify that the displacements of the EP and superstructure and the axial loads remain within admissible limits. Furthermore, the efficiency is related to the amount of thermal energy that can be exchanged with the ground.

Although the THM model can evaluate the variations in pore water pressure due to the heat-transfer processes, they are not analysed in the present study because Adinolfi *et al.* (2018) showed that the increases/decreases in pore water pressure during heating/cooling are negligible for the safety of the building.

Behaviour of EP in current and future time spans

The depth profiles are shown in Figure 5. The analysed time steps correspond to the end of the mechanical phase of cooling (C) and of heating (H) and the end of the simulation (E) when the temperature is again kept constant at T_{ref} and the mechanical load is still 1000 kN on the pile head.

The vertical displacements are evaluated along the pile axis. In accordance with the thermally induced expansion/contraction of the pile, the upper part of the pile moves upwards during heating and downwards during cooling, while the pile toe does the opposite. Figure 5(a) shows that because of the stiffness of the soil, the displacements induced by the thermo-mechanical loads on the EP, in all scenarios, are far from being detrimental to the building, ranging from −2.00 to −0.70 mm. The null point, characterised by zero thermally induced displacement, appears at a pile depth-to-length ratio of around 0.77. Because of the mechanical load, the pile head and toe settle by around −1.4 and −0.9 mm, respectively. In this configuration, the EP works in cooling mode with an additional downward displacement, and the maximum settlement (−2 mm) of the EP head is reached with RCP 8.5. Then, in heating mode, the EP head moves in the opposite sense, reducing the settlement to −1.1 mm with RCP 8.5 (the existing settlement in the paper by Adinolfi *et al.* (2018) is up to −0.8 mm). At stage E, the vertical displacement profile approaches the initial one: residual displacements are due to consolidation processes and plasticity effects. The vertical displacements agree with the temperature changes (Figure 5(c)). The axial load paths are shown in Figure 5(b). As expected, the EP under only mechanical load exhibits a compressive profile

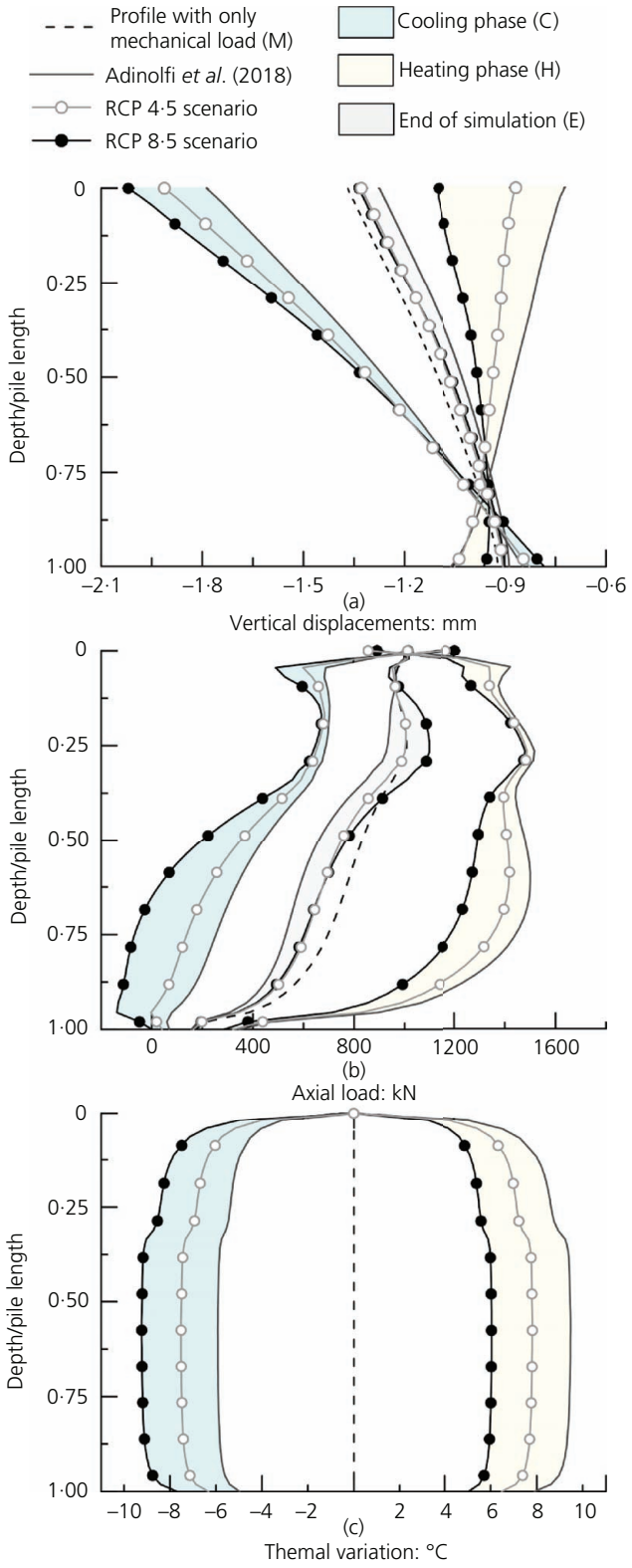

Figure 5. Performances of EP (adopted sign convention is positive for compressive axial load and negative for settlements): (a) vertical displacements along the pile axis; (b) axial loads; (c) temperature variation profiles at the soil–pile interface

(dotted line): the largest part of the mechanical load is supported by shaft friction, and only a small portion is transmitted at the pile tip (~200 kPa). Although the mechanical load is responsible for mobilising the majority of the interfacial shear stress, the thermal variations (Figure 5(c)) induce additional shear stresses in both the upward and downward directions, particularly under RCP 8.5 and cooling mode. In such a case, the EP is less compressed than it is with the current and RCP 4.5 profiles, reaching tensile values of up to −140 kN in the lower part (at a pile depth-to-length ratio of 0.66 and down to EP toe). Previous results (Adinolfi *et al*., 2018) show the compressive stress increasing after the heating phase, with the maximum compressive axial load of 1500 kN (at a pile depth-to-length ratio of 0.60) where the induced shear stresses reverse from downwards to upwards. Scenarios RCP 4.5 and RCP 8.5 entail lower values of axial load than those assessed in the current conditions. Peak values are also observed at a pile depth-to-length ratio of 0.33, corresponding to a depth of 3.5 m, at the contact between the pozzolanas and tuff layers. So, regarding structural safety of the proposed EP in Naples, additional thermal compressive as tough tensile stresses due to CC under scenarios RCP 4.5 and RCP 8.5, do not represent a significant risk for the performance of the foundation.

The temperature profiles (variations with respect to the initial reference temperature) at the soil–pile interface are shown in Figure 5(c): the plots highlight the differences between the start of the simulations and the end of both the heating and cooling periods, with a consequent gain in terms of pile–ground heat transfer. The temperature is almost uniform along the EP shaft. At the upper boundary of the domain, the variation is zero because T_{ref} is imposed as both a boundary condition and an initial constant temperature. After the cooling phase, the temperature decreases by −5.0°C (following the ED from the paper by Adinolfi *et al*. (2018)), −7.0°C (following the ED for RCP 4.5) and −9.0°C (following the ED for RCP 8.5). At the end of heating, the temperature increases by +6.0°C (following the ED for RCP 8.5), +8°C (following the ED for RCP 4.5) and +9°C (following the ED from the paper by Adinolfi *et al*. (2018)) with respect to the respective T_{ref}. The projection under the RCP 8.5 scenario, in terms of thermal benefits, suggests that the maximum thermal exchange between the ground and the EP occurs in cooling (winter), while a lower amount of energy than the existing results is extracted from the ground after heating (summer).

Note that the scenarios differ in two main effects – namely, the soil temperature and the ED. Although the cooling phase of the ED (Figure 3(c)) reduces with RCP 8.5, the maximum thermal exchanges with the ground are assessed after cooling because the soil temperature is set to 20.9°C and the temperature into the probes is 10°C. In contrast, the duration of the heating demand (Figure 3(c)) in the RCP 8.5 scenario is less than in the others, so the minimum thermal exchange is realised with the ground (the soil temperature is set to 20.9°C and that into the probes is 28°C). Further analyses (Appendix 3) are aimed at decoupling the effects. It results that soil temperature is the main influent factor on the EP performance coped with CC.

Effects of thermo-mechanical cycle in pile and surrounding soil

Figure 6 shows the annual mechanical and thermal cycles of the EP and surrounding soil in terms of time series of vertical displacements, axial loads and temperature. The investigated points are at the pile head (A) and on the pile axis at depths of 2.5 m (B) and 7.5 m (C). There are also points in the surrounding soil: in the tuff stratum at a depth of 7.5 m at distances of 1.0 m (D) and 2.0 m (E) from the pile shaft and in the pozzolana stratum at a depth of 2.5 m at distances of 2.0 m (F) and 1.0 m (G) from the pile shaft. The time histories of the vertical displacements (positive upwards) of the EP and soil are presented in Figures 6(a), 6(d) and 6(g). Generally, the evolutions in the upper domain are qualitatively similar but more marked for the points on the pile shaft (A, B), which are subjected to a higher temperature variation (Figure 3(b)) than are points G and F in the soil. Indeed, the lower points (C at the pile toe, D and E in the tuff stratum) move, albeit undetectably, downwards during heating and upwards during cooling, behaving as expected in the opposite manner to the upper part of the pile. Regarding the mechanically induced displacements, the cooling phase generates displacements that are lower than the mechanical ones, while the heating phase induces higher displacements. Regarding safety, scenario RCP 8.5 increases the pile displacements by around 10% (points A–C) with respect to the current behaviour in cooling mode, but nevertheless the ED in such a phase lasts for less time than it does

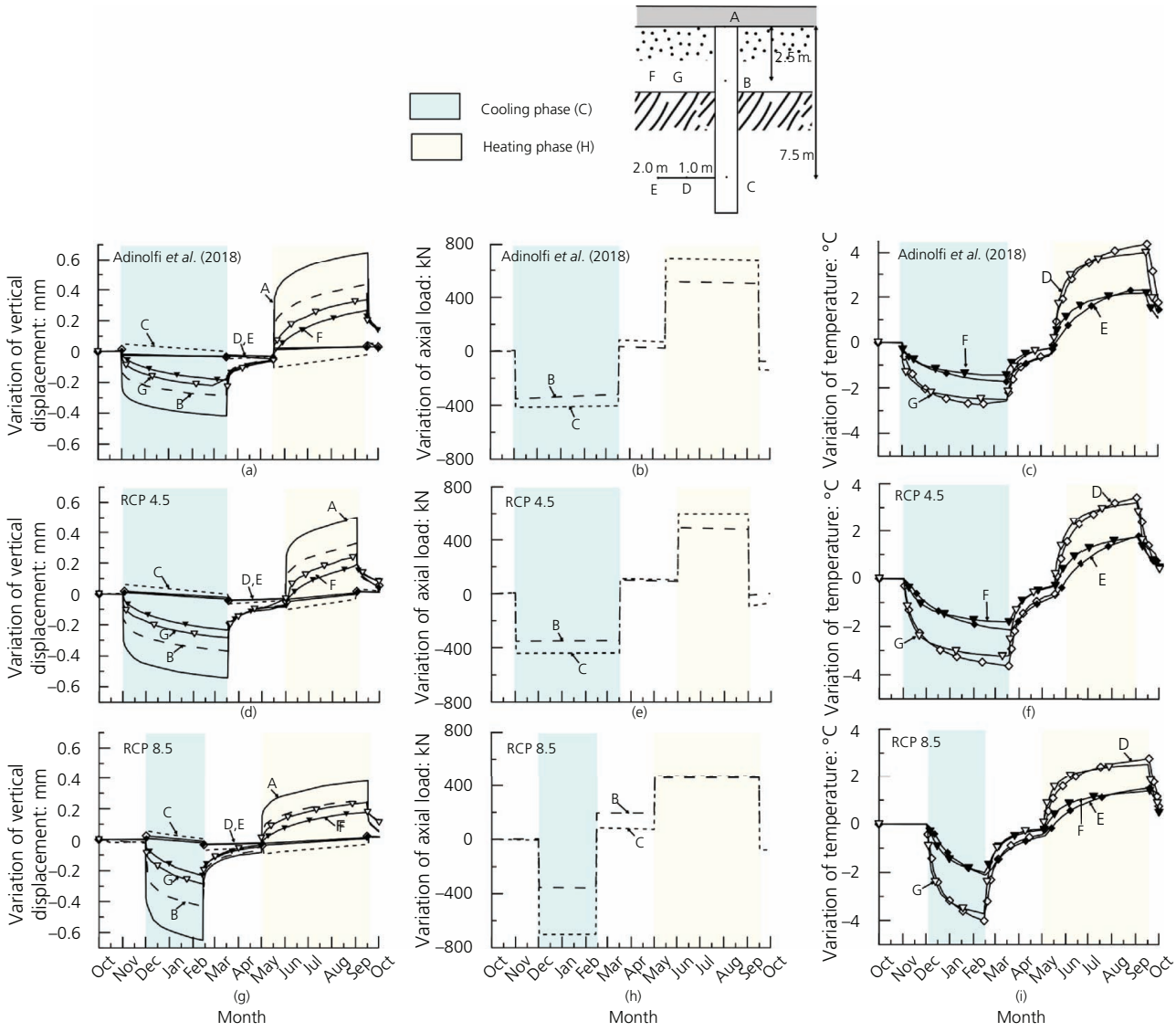

Figure 6. Time histories of vertical displacements following the (a) ED from the paper by Adinolfi *et al*. (2018), (d) ED for RCP 4.5 and (g) ED for RCP 8.5. Time histories of axial loads along pile (points B and C) following the (b) ED from the paper by Adinolfi *et al*. (2018), (e) ED for RCP 4.5 and (h) ED for RCP 8.5. Time histories of temperature following the (c) ED from the paper by Adinolfi *et al*. (2018), (f) ED for RCP 4.5 and (i) for ED RCP 8.5. Investigated points are along the pile axis (points A, B and C) and in surrounding soils (points D, E, F and G)

in other cases. The magnitudes of the displacements in the surrounding soil (points D–G) in both future scenarios remain close to the current ones.

The mechanical effects that the thermal behaviour induces in the pile were also assessed from the time evolution of the axial load at points B and C. The curves in Figure 6(b), 6(e) and 6(h) represent the axial load variation with respect to the initial value but due only to the applied mechanical load. The results show clearly that the deformations associated with the temperature variations decrease (increase) the axial load in the EP by −400 kN (700 kN). The axial load variations decrease in cooling mode under RCP 8.5 (Figure 6(h)), with variations of around 70% of those in the current behaviour (Figure 6(b)), this being due to the higher thermal exchange (Figure 3(c)) and the shorter duration of the ED in cooling mode. In heating mode, the RCP scenarios show reducing axial load variations compared with current behaviour (Figure 6(b)). In all cases, the deeper point (C) is more stressed than the upper one (B).

The time histories of the temperature in the surrounding soil (that of the inner pile is close to the ED) are shown in Figures 6(c), 6(f) and 6(i) for points D–G. In both RCP scenarios and in the current behaviour, the thermal behaviour induces a temperature increase/decrease of less than 4°C in the surrounding soil. The temperature variations are more significant at 1.0 m from the pile (points D and G) than they are at 2.0 m (points E and F).

Discussion and conclusions

The main goal of the present work was to analyse the geotechnical performance of an EP accounting for expected CC. The city of Naples was considered as the study area, and the long-term performance of the EP was evaluated over the future period of 2071–2100 under the RCP 4.5 and RCP 8.5 scenarios and was compared with the existing results of Adinolfi *et al*. (2018). The scenarios differ mainly with regard to soil temperature and ED. A THM model was used to understand the behaviour of the EP. The key points and conclusions of the present study are discussed in the following.

Climate projections give increases in the outdoor near-surface air temperatures in Naples of around 2 and 4°C with RCP 4.5 and RCP 8.5, respectively. The same increases can be expected for the average ground temperature. However, because of uncertainties in future trends, such investigations should be conducted in future work by exploiting ensemble projections, thereby permitting a proper and quantitative evaluation.

Because of increasing outdoor temperature, the ED of the building in terms of consumption for heating during winter and air-conditioning during summer could be strongly affected in the future. The present paper proposes a novel approach based on HDD and CDD thresholds that allows the ED to be defined accounting for the activity time of the GSHP system and the duration of extraction/injection from/into the ground (cooling/heating phase for the pile–soil system) with RCP 4.5 and RCP 8.5. Specifically, the energy extraction during winter (cooling phase) will reduce in duration in the future scenarios, particularly under RCP 8.5. Meanwhile, the ED of air-conditioning the building during summer, corresponding to the heating phase, increases, particularly with RCP 8.5. In future projections, EPs and EGs in general are expected to satisfy the increasing air-conditioning requirements of buildings.

Regarding the geotechnical performance, the results confirm that when the EP is subjected to a temperature variation, part of the thermal deformation of the pile is prevented, thereby generating additional compressive and tensile stresses during heating and cooling, respectively. The pile reacts to the induced thermal exchange, showing an upwards head displacement during heating and a downwards one during cooling. The maximum pile head displacement is −2.0 mm for the RCP 8.5 scenario, far from being detrimental to the overlying building. This maximum settlement is approximately 10% higher than the existing one (Adinolfi *et al*., 2018) and is 38% of the mechanically induced one. The surrounding soil exhibits no further significant thermally induced displacement, and the future scenarios give a behaviour that is close to the current one (Adinolfi *et al*., 2018).

As the maximum thermal exchange after the cooling phase is performed with RCP 8.5, additional and notable tensile stresses (around +70%) are generated at the pile toe. In contrast, because of the reduced thermal exchange after the heating phase with RCP 8.5, the compressive axial load profiles decrease in future scenarios. To resist the uplift forces, greater EP reinforcement is required as an adaptation strategy, expecting in future spans a reduction in compressive axial load and vertical displacement in heating mode and an increase in pile head settlement and tensile stress during cooling. Although the present results are specific to the case study and depend on assumptions, soil properties and the applied mechanical and thermal loads, negligible interference with the structural capacity of EP in terms of pile head displacements and axial loads are exploited, highlighting negligible geotechnical risk and serviceability problems for the upper structure.

The findings in terms of temperature exchanges from/into the ground underline that on the long time horizon of 2071–2100, the EP moves towards maximum thermal exchanges during winter and low thermal gains during summer. RCP 8.5 projects a thermal exchange of 9°C after cooling and 6°C after heating, and the effects of thermal exchange are felt in the surrounding soil up to a distance of 2.0 m from the pile.

The presence of an overlying structure above the EP could impose a constant initial temperature on the soil–pile system. This effect is considered in the numerical analyses of Appendix 3, resulting in a decoupling of the effects of the soil temperature and the ED factors addressed by CC. It is detected that the main factor influencing the EP performance is T_{ref}, while the difference in the durations of the cooling and heating phases in the ED has less influence on the EP performance.

The present findings provide insight into the behaviour of EPs with particular emphasis on CC influences on both the thermal and geotechnical performances. These aspects must be considered carefully in the future development of the EG technologies and could support communities, designers and decision makers.

Appendix 1

The evaluation of future variations in atmospheric patterns under CC exploits a well-consolidated simulation chain (Wilby, 2017), with the following stages adopted in cascade.

(*a*) Future releases into the atmosphere of GHGs, aerosols and other pollutants are estimated by means of socio-economic integrated assessment models. Such models permit the identification of concentration 'pathways' associated with several assumptions concerning demographic variations, land use changes, gross domestic products, and socio-economic and technological development. IPCC (2014) proposed the RCP scenarios, developed in the framework of the Fifth Coupled Model Intercomparison Project (Taylor *et al*., 2012). In particular, the RCP 2.6, RCP 4.5, RCP 6.0 and RCP 8.5 scenarios (Moss *et al*., 2010) have been identified, where the suffix stands for the expected increase in radiative forcing in 2100 compared with that in the pre-industrial era (1750). Of course, RCP 2.6 is the most optimistic scenario; RCP 4.5 and RCP 6.0 (Thomson *et al*., 2011) are midway-stabilisation scenarios; and, finally, RCP 8.5 (Riahi *et al*., 2011) is a high-concentration scenario but business as usual. Furthermore, only RCP 2.6 is assessed at the global scale, permitting address of the Paris target for maintaining increases in temperature under 1.5°C.

(*b*) RCPs are used to force GCMs, which are physically based numerical models that reproduce the processes that regulate the general circulation of the atmosphere on a global scale. As shown by Wilby (2017), strong increases in computational power allowed a significant increase in the permitted horizontal resolution (from ~500 km in the 1970s to 50–80 km nowadays) while accounting for more complex physical and atmospheric dynamics (e.g. carbon cycle and atmospheric chemistry). From this perspective, GCMs are usually known as Earth system models. Nevertheless, they return details about global patterns but are inadequate for local atmospheric dynamics, thereby preventing their direct adoption for impact studies (becoming 'policy-relevant climate projections').

(*c*) To cope with that issue, statistical or dynamical downscaling approaches are usually adopted. The former retrieve relationships among large-scale and local atmospheric variables based on available observations/results for the current period. They are cost and time effective, but because they are usually adopted at point scale, they require long observation data sets for calibration and validation (Maraun and Widmann, 2018). The latter are numerical atmospheric models called regional climate models (RCMs) nested from a GCM (used as initial and boundary conditions) on the area of interest. They permit horizontal resolutions of up to a few kilometres, allowing the reproduction of very local atmospheric patterns associated with orography or urban environments. Nevertheless, they require significant time and computational resources.

(*d*) However, despite the increases in resolution permitted by RCMs, comparisons with point-scale and gridded observed data sets usually detect remaining biases, thereby preventing the adoption of such outputs as inputs to impact models. To cope with such constraints, several approaches have been proposed involving statistical post-processing to adjust the model outputs towards observations (Maraun and Widmann, 2018). In the simplest approaches, atmospheric variables are adjusted by accounting for mean biases retrieved comparing observations and simulations on the current reference period (delta approach). Nevertheless, it is well recognised (Lafon *et al*., 2013) that the biases could have different magnitudes according to the considered quantile. In this perspective, quantile mapping approaches have been introduced where 'a quantile of the present day simulated distribution is replaced by the same quantile of the present-day observed distribution', and the same rule is exploited for future projections (Maraun, 2016).

Atmospheric variables provided by such simulation chains can finally be adopted as input for impact tools (statistical or physically based). To manage uncertainties associated with the different components of simulation chains, ensemble approaches are usually adopted (Rianna *et al*., 2017). According to the ensemble approaches, the exploitation of different simulations allows the identification of uncertainties associated with estimated variations. In this regard, key international initiatives such as the Coordinated Regional Downscaling Experiment (Cordex, 2020) programmes make available findings provided by several RCMs on fixed domains and grid resolution, thereby permitting much easier comparison among the results.

Appendix 2

A THM coupled formulation is used in numerical simulations of a single EP in Naples, subjected to (*a*) a constant mechanical load and (*b*) thermal loads given by a long-term 400 d ED. The governing equations – reproducing the mechanical behaviour of the solid skeleton, the heat conduction and convection and the hydraulic flow in the soil – are solved taking into account the following assumptions: (*a*) The soil is considered as a bi-phase dry material (solid and air) above the groundwater table and a fully saturated bi-phase mass (solid and water) below it. It is modelled as isotropic and linear elastic–perfectly plastic materials with a Drucker–Prager yield surface, the size of which is defined by matching it with the Mohr–Coulomb criterion in compressive tests. (*b*) The pile is modelled as an isotropic thermo-elastic non-porous material. (*c*) Perfect contact between the soil and the pile is assumed. (*d*) The displacements and deformations of the solid skeleton are small (linear kinematics). (*e*) The effective stress principle is considered. (*f*) The fluid phase and the soil grains are incompressible.

The set of governing equations following the model proposed by Adinolfi *et al.* (2018) is used, taking into account the preceding hypotheses. For the equilibrium considerations, the divergence of the total stress tensor is balanced by the vector of external forces – namely

$$4. \quad \nabla\boldsymbol{\sigma} + \boldsymbol{b} = 0$$

where $\boldsymbol{\sigma}$ is the total stress tensor (axial stresses are positive if tensile) and $\boldsymbol{b}$ is the volume external force vector due to the gravity loads, which takes into account the soil density ρ, depending on the soil porosity, the fluid density and the solid-particle density. The thermal elastic Hooke's law for porous material, with the hydro-mechanical coupling of the effective stress, becomes

$$5. \quad \boldsymbol{\sigma} = \boldsymbol{D}^e\left(\boldsymbol{\varepsilon} - \boldsymbol{\varepsilon}^T - \boldsymbol{\varepsilon}_{\mathrm{pl}}\right) - p\boldsymbol{I}$$

where $\boldsymbol{D}^{\mathrm{e}}$ is the elastic stiffness tensor; $\boldsymbol{\varepsilon}$ is the strain tensor; $\boldsymbol{\varepsilon}^{\mathrm{T}}$ is the thermal strain tensor; $\boldsymbol{\varepsilon}_{\mathrm{pl}}$ is the plastic strain tensor; p is the pore water pressure (positive if compressive); and $\boldsymbol{I}$ is the second-order unit tensor. Plastic deformations are computed by the constitutive model of the Drucker–Prager yield criterion, while free axial thermal deformations are computed by means of Equation 6 and accounting for the volumetric axial thermal expansion coefficient α_{s} of the material (pile concrete and solid skeleton) and the temperature variation ΔT

$$6. \quad \boldsymbol{\varepsilon}^T = 1/3(\alpha_{\mathrm{s}}\Delta T)\boldsymbol{I}$$

Mass conservation is expressed as

$$7. \quad \rho\frac{\partial\varepsilon_{\mathrm{vol}}}{\partial t} + \nabla(\rho_{\mathrm{w}}\boldsymbol{v}) - \rho\beta_{\mathrm{sw}}\frac{\partial T}{\partial t} = 0$$

where $\varepsilon_{\mathrm{vol}}$ is the volumetric strain; t is time; T is the temperature; and β_{sw} is the volumetric thermal expansion of the bi-phase mass that takes into account α_{w} for water and α_{s} for the solid skeleton – namely

$$8. \quad \beta_{\mathrm{sw}} = (1-n)\alpha_{\mathrm{s}} + n\alpha_{\mathrm{w}}$$

In Equation 7, $\boldsymbol{v}$ is the relative velocity vector of the water following the Darcy's law, depending on the hydraulic conductivity tensor $\boldsymbol{K}$ that is a function of the permeability of the porous media (temperature independent) and of the density and the dynamic viscosity of the water, which are temperature dependent (thermo-hydraulic coupling).

Conservation of energy for the porous media is expressed as

$$9. \quad (\rho c)_{\mathrm{eq}}\frac{\partial T}{\partial t} + \rho_{\mathrm{w}}c_{\mathrm{w}}\nabla(T\boldsymbol{v}) - \boldsymbol{\lambda}_{\mathrm{eff}}\nabla^2 T = 0$$

where ∇^2 is the Laplace operator; $\boldsymbol{\lambda}_{\mathrm{eff}}$ is the thermal conductivity tensor of the soil; c is the soil specific heat capacity; c_{s} and c_{w} are the solid-skeleton and water specific heat capacities, respectively; and $(\rho c)_{\mathrm{eq}}$ is the volumetric heat capacity of saturated soil. In Equation 9, the first term represents the energy stored in the medium, the second one the energy transported by convection (thermo-hydraulic coupling) and the third one the heat transferred by conduction (Fourier's law).

Appendix 3

The proper thermal upper boundary condition is a key issue in numerical studies of EPs. The literature suggests several approaches regarding the surface temperature condition, gathered in the work of Bourne-Webb *et al.* (2019). In particular, (*a*) some numerical studies (Bodas Freitas *et al.*, 2013; Rotta Loria and Laloui, 2016) assumed adiabatic conditions at the upper boundary, neglecting any influence from the overlying structure and/or external environment; (*b*) other numerical studies (Brandl, 2006; Jeong *et al.*, 2014; Olgun *et al.*, 2015; Sani *et al.*, 2019; Suryatriyastuti *et al.*, 2012) assumed that the ground surface temperature is governed by the daily mean air temperature; and (*c*) some others (Di Donna and Laloui, 2015; Dupray *et al.*, 2014; Gawecka *et al.*, 2018; Salciarini *et al.*, 2012, 2015) assumed a constant temperature at the upper bound connected with the overlying structure.

The present research is based on approach (*b*). In the view of CC, that approach could be considered to be the most challenging because global warming is expected to affect both ground temperature and ED. Anyway, the presence of an overlying building in an urban environment could modify the heat exchange between the atmosphere and the ground. Many field studies (Ferguson and Woodbury, 2007; Thomas and Rees, 1998; Zhu *etal.*, 2010) have shown that a small heat flux may exist between the urban environment and the ground.

To account for the presence of the building, following the literature cited for approach (*c*), an increase in temperature of at least 4°C (Dupray *et al.*, 2014) with respect to the expected temperature without an overlying structure should be applied as the initial ground temperature. In this perspective, additional analyses are proposed in which an initial temperature of 20.9°C was used as T_{ref} and only the ED varies, addressed by CC. There are three assessed simulations: the first uses the ED from the paper by Adinolfi *et al.* (2018) and T_{ref} = 20.9°C as the initial soil temperature; the second uses RCP 4.5 as the ED and T_{ref} = 20.9°C; and the third runs with RCP 8.5 and T_{ref} = 20.9°C, the same as presented in the section entitled 'Performance of EP in Naples'.

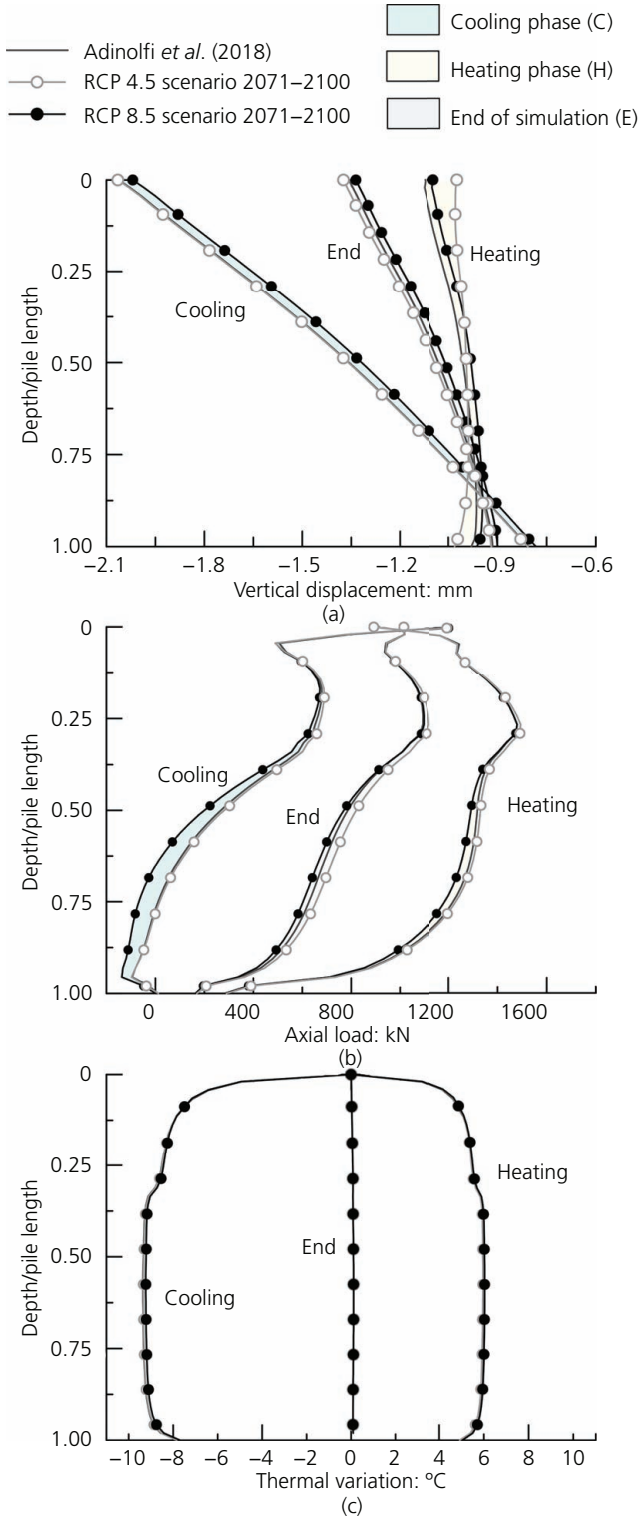

Figure 7. Performances of EP (adopted sign convention is positive for compressive axial load and negative for settlements) with initial temperature T_{ref} = 20.9°C: (a) vertical displacements along the pile axis; (b) axial loads; (c) temperature profiles at the soil–pile interface

The performances of the EP are shown in Figure 7.

The results of the proposed simulations show profiles that are close to each other but with slight differences due to the different durations of heating and cooling phases in the ED. The presence of the building induces almost the same thermal exchange. Such analyses, if compared with those of Figure 5, allow decoupling the effects on EP of CC influence on both ground temperature and ED. Indeed, in Figure 7, only the EDs vary driven by CC (i.e. the different durations of the cooling and heating phases). From comparing Figures 5 and 7, note that the main influencing factor in EP technology, affected by CC, is the initial soil temperature T_{ref}, whereas ED is less influential on the EP performance.

Acknowledgements

The authors would like to thank the REM (Regional Models) and SDC (Statistical Downscaling & CLIME) units of Remhi (Regional Models and Geo-Hydrological Impacts) of the Euro-Mediterranean Center on Climate Change (CMCC) Foundation for their essential support in providing the preprocessed climate data used in the present work.

REFERENCES

Adinolfi M, Mauro A, Maiorano RMS, Massarotti N and Aversa S (2016) Thermo-mechanical behaviour of energy pile in underground railway construction site. In *Energy Geotechnics: Proceedings of the 1st International Conference on Energy Geotechnics, ICEGT 2016, Kiel, Germany, 29–31 August 2016* (Wuttke F, Bauer S and Sanchez M (eds)). CRC Press/Balkema, Leiden, the Netherlands, pp. 83–90.

Adinolfi M, Maiorano RMS, Mauro A, Massarotti N and Aversa S (2018) On the influence of thermal cycles on the yearly performance of an energy pile. *Geomechanics for Energy and the Environment* **16**: 32–44, https://doi.org/10.1016/j.gete.2018.03.004.

Badenes B, Magraner T, De Santiago C *et al.* (2017) Thermal behaviour under service loads of a thermo-active precast pile. *Energies* **10(9)**: article 1315, https://doi.org/10.3390/en10091315.

Bayer P, Rivera JA, Schweizer D *et al.* (2016) Extracting past atmospheric warming and urban heating effects from borehole temperature profiles. *Geothermics* **64**: 289–299, https://doi.org/10.1016/j.geothermics.2016.06.011.

Bodas Freitas T, Cruz Silva F and Bourne-Webb P (2013) The response of energy foundations under thermo-mechanical loading. *Proceedings of the 18th International Conference on Soil Mechanics and Geotechnical Engineering, Paris, France*, vol. 4, pp. 3347–3350.

Bourne-Webb PJ, Amatya B, Soga K *et al.* (2009) Energy pile test at Lambeth College, London: geotechnical and thermodynamic aspects of pile response to heat cycles. *Géotechnique* **59(3)**: 237–248, https://doi.org/10.1680/geot.2009.59.3.237.

Bourne-Webb P, Burlon S, Javed S, Kürten S and Loveridge F (2016) Analysis and design methods for energy geostructures. *Renewable and Sustainable Energy Reviews* **65**: 402–419, https://doi.org/10.1016/j.rser.2016.06.046.

Bourne-Webb PJ, Freitas TB and Assunção RF (2019) A review of pile–soil interactions in isolated, thermally-activated piles. *Computers and Geotechnics* **108**: 61–74, https://doi.org/10.1016/j.compgeo.2018.12.008.

Brandl H (2006) Energy foundations and other thermo-active ground structures. *Géotechnique* **56(2)**: 81–122, https://doi.org/10.1680/geot.2006.56.2.81.

Bucchignani E, Montesarchio M, Zollo AL and Mercogliano P (2016) High-resolution climate simulations with COSMO-CLM over Italy:

performance evaluation and climate projections for the 21st century. *International Journal of Climatology* **36(2)**: 735–756, https://doi.org/10.1002/joc.4379.

Burger A (1985) *Thermique des Nappes Souterraines*. Presses Polytechniques Romandes, Lausanne, Switzerland (in French).

Cordex (Coordinated Regional Downscaling Experiment) (2020) http://www.cordex.org (accessed 28/03/2020).

De Santiago C, de Santayana FP, De Groot M *et al.* (2016) Thermo-mechanical behavior of a thermo-active precast pile. *Bulgarian Chemical Communications* **48**: 41–54.

Di Donna A and Barla M (2016) The role of ground conditions on energy tunnels' heat exchange. *Environmental Geotechnics* **3(4)**: 214–224, https://doi.org/10.1680/jenge.15.00030.

Di Donna A and Laloui L (2015) Numerical analysis of the geotechnical behaviour of energy piles. *International Journal for Numerical and Analytical Methods in Geomechanics* **39(8)**: 861–888, https://doi.org/10.1002/nag.2341.

Dupray F, Laloui L and Kazangba A (2014) Numerical analysis of seasonal heat storage in an energy pile foundation. *Computers and Geotechnics* **55**: 67–77, https://doi.org/10.1016/j.compgeo.2013.08.004.

Ferguson G and Woodbury AD (2007) Urban heat island in the subsurface. *Geophysical Research Letters* **34(23)**: L23713, https://doi.org/10.1029/2007GL032324.

Gawecka KA, Potts DM, Cui W, Taborda DM and Zdravković L (2018) A coupled thermo-hydro-mechanical finite element formulation of one-dimensional beam elements for three-dimensional analysis. *Computers and Geotechnics* **104**: 29–41, https://doi.org/10.1016/j.compgeo.2018.08.005.

Gudmundsson L, Bremnes JB, Haugen JE and Engen-Skaugen T (2012) Downscaling RCM precipitation to the station scale using statistical transformations: a comparison of methods. *Hydrology and Earth System Sciences* **16(9)**: 3383–3390, https://doi.org/10.3929/ethz-b-000058274.

Hillel D (2012) *Soil and Water: Physical Principles and Processes*. Elsevier, St Louis, MO, USA.

IPCC (Intergovernmental Panel on Climate Change) (2014) *Climate Change 2014: Synthesis Report. Contribution of Working Groups I, II and III to the Fifth Assessment Report of the Intergovernmental Panel on Climate Change* (Core Writing TeamPachauri RK, Meyer LA (eds)). IPCC, Geneva, Switzerland.

Jeong S, Lim H, Lee K and Kim J (2014) Thermally induced mechanical response of energy piles in axially loaded pile groups. *Applied Thermal Engineering* **71**: 608–615, https://doi.org/10.1016/j.applthermaleng.2014.07.007.

Lafon T, Dadson S, Buys G and Prudhomme C (2013) Bias correction of daily precipitation simulated by a regional climate model: a comparison of methods. *International Journal of Climatology* **33(6)**: 1367–1381, https://doi.org/10.1002/joc.3518.

Laloui L, Nuth M and Vulliet L (2006) Experimental and numerical investigations of the behaviour of a heat exchanger pile. *International Journal for Numerical and Analytical Methods in Geomechanics* **30(8)**: 763–781, https://doi.org/10.1002/nag.499.

Lee CC and Chiu YB (2011) Electricity demand elasticities and temperature: evidence from panel smooth transition regression with instrumental variable approach. *Energy Economics* **33(5)**: 896–902, https://doi.org/10.1016/j.eneco.2011.05.009.

Maraun D (2016) Bias correcting climate change simulations – a critical review. *Current Climate Change Reports* **2**: 211–220, https://doi.org/10.1007/s40641-016-0050-x.

Maraun D and Widmann M (2018) *Statistical Downscaling and Bias Correction for Climate Research*. Cambridge University Press, Cambridge, UK.

Menberg K, Blum P, Schaffitel A and Bayer P (2013) Long-term evolution of anthropogenic heat fluxes into a subsurface urban heat island. *Environmental Science & Technology* **47(17)**: 9747–9755, https://doi.org/10.1021/es401546u.

Moss RH, Edmonds JA, Hibbard KA *et al.* (2010) The next generation of scenarios for climate change research and assessment. *Nature* **463(7282)**: 747–756, https://doi.org/10.1038/nature08823.

Oke TR, Mills G and Voogt JA (2017) *Urban Climates*. Cambridge University Press Cambridge, UK.

Olgun CG, Ozudogru TY, Abdelaziz SL and Senol A (2015) Long-term performance of heat exchanger piles. *Acta Geotechnica* **10(5)**: 553–569, https://doi.org/10.1007/s11440-014-0334-z.

Ozudogru TY, Olgun CG and Arson CF (2015) Analysis of friction induced thermo-mechanical stresses on a heat exchanger pile in isothermal soil. *Geotechnical and Geological Engineering* **33**: 357–371, https://doi.org/10.1007/s10706-014-9821-0.

Riahi K, Rao S, Krey V *et al.* (2011) RCP 8.5 – a scenario of comparatively high greenhouse gas emissions. *Climatic Change* **109(1–2)**: article 33, https://doi.org/10.1007/s10584-011-0149-y.

Rianna G, Reder A, Mercogliano P and Pagano L (2017) Evaluation of variations in frequency of landslide events affecting pyroclastic covers in Campania region under the effect of climate changes. *Hydrology* **4(3)**: article 34, https://doi.org/10.3390/hydrology4030034.

Rivera JA, Blum P and Bayer P (2017) Increased ground temperatures in urban areas: estimation of the technical geothermal potential. *Renewable Energy* **103**: 388–400, https://doi.org/10.1016/j.renene.2016.11.005.

Rockel B, Will A and Hense A (2008) The regional climate model COSMO-CLM (CCLM). *Meteorologische Zeitschrift* **17(4)**: 347–348.

Rotta Loria AF and Laloui L (2016) Thermally induced group effects among energy piles. *Géotechnique* **67(5)**: 374–393, https://doi.org/10.1680/jgeot.16.P.039.

Rotta Loria AF and Laloui L (2017) The equivalent pier method for energy pile groups. *Géotechnique* **67(8)**: 691–702, https://doi.org/10.1680/jgeot.16.P.139.

Rotta Loria AF and Laloui L (2018) Thermo-mechanical schemes for energy piles. In *Energy Geotechnics: SEG-2018* (Ferrari A and Laloui L (eds)). Springer, Cham, Switzerland, pp. 218–225.

Salciarini D, Tamagnini C and Cinfrignini E (2012) Modellazione dei processi termo-idro-meccanici indotti in prossimita di pali geotermici. *Proceedings of the 2012 Incontro Annuale dei Ricercatori di Geotecnica. Padua, Italy* (in Italian).

Salciarini D, Ronchi F, Cattoni E and Tamagnini C (2015) Thermo-mechanical effects induced by energy piles operation in a small piled raft. *International Journal of Geomechanics* **15(2)**: article 04014042, https://doi.org/10.1061/(ASCE)GM.1943-5622.0000375.

Sani K, Singh RM, Amis T and Cavarretta I (2019) A review on the performance of geothermal energy pile foundation, its design process and applications. *Renewable and Sustainable Energy Reviews* **106**: 54–78, https://doi.org/10.1016/j.rser.2019.02.008.

Scapin S, Apadula F, Brunetti M and Maugeri M (2016) High-resolution temperature fields to evaluate the response of Italian electricity demand to meteorological variables: an example of climate service for the energy sector. *Theoretical and Applied Climatology* **125(3–4)**: 729–742, https://doi.org/10.1007/s00704-015-1536-5.

Scoccimarro E, Gualdi S, Bellucci A *et al.* (2011) Effects of tropical cyclones on ocean heat transport in a high-resolution coupled general circulation model. *Journal of Climate* **24(16)**: 4368–4384, https://doi.org/10.1175/2011JCLI4104.1.

Spinoni J, Vogt J and Barbosa P (2015) European degree-day climatologies and trends for the period 1951–2011. *International Journal of Climatology* **35(1)**: 25–36, https://doi.org/10.1002/joc.3959.

Suryatriyastuti ME, Mroueh H and Burlon S (2012) Understanding the temperature-induced mechanical behaviour of energy pile foundations. *Renewable and Sustainable Energy Reviews* **16(5)**: 3344–3354, https://doi.org/10.1016/j.rser.2012.02.062.

Taylor KE, Stouffer RJ and Meehl GA (2012) An overview of CMIP5 and the experiment design. *Bulletin of the American Meteorological Society* **93**: 485–498, https://doi.org/10.1175/BAMS-D-11-00094.1.

Thomas HR and Rees SW (1998) The thermal performance of ground floor slabs – a full scale in-situ experiment. *Building and Environment* **34(2)**: 139–164, https://doi.org/10.1016/S0360-1323(98)00001-8.

Thomson AM, Calvin KV, Smith SJ *et al.* (2011) RCP4.5: a pathway for stabilization of radiative forcing by 2100. *Climatic Change* **109(1–2)**: article 77, https://doi.org/10.1007/s10584-011-0151-4.

UK Met Office (2013) http://www.metoffice.gov.uk/ (accessed 28/03/2020).

Villani V, Rianna G, Mercogliano P and Zollo AL (2015) Statistical approaches versus weather generator to downscale RCM outputs to slope scale for stability assessment: a comparison of performances. *Electronic Journal of Geotechnical Engineering* **20(4)**: 1495–1515.

Wilby RL (2017) *Climate Change in Practice: Topics for Discussion with Group Exercises*. Cambridge University Press, Cambridge, UK.

Zhang Y, Choudhary R and Soga K (2015) Influence of GSHP system design parameters on the geothermal application capacity and electricity consumption at city-scale for Westminster, London. *Energy and Buildings* **106**: 3–12, https://doi.org/10.1016/j.enbuild.2015.07.065.

Zhu K, Blum P, Ferguson G, Balke KD and Bayer P (2010) The geothermal potential of urban heat islands. *Environmental Research Letters* **5(4)**: article 044002.

Zollo AL, Rianna G, Mercogliano P, Tommasi P and Comegna L (2014) Validation of a simulation chain to assess climate change impact on precipitation induced landslides. In *Landslide Science for a Safer Geoenvironment: Volume 1 – the International Programme on Landslides (IPL)* (Sassa K, Canuti P and Yin Y (eds)). Springer, Cham, Switzerland, pp. 287–292.